Deformation Properties of Single Red Blood Cell in a Stenosed Microchannel

P.G.H. Nayanajith[1], S. C. Saha[1], and Y.T. Gu[1]*

[1]School of Chemistry, Physics and Mechanical Engineering
Queensland University of Technology, Brisbane, Queensland, Australia

*Corresponding author: yuantong.gu@qut.edu.au

Abstract

Red Blood Cells (RBCs) exhibit different types of motions and different deformed shapes, when they move through capillaries. RBCs can travel through capillaries having smaller diameters than RBCs' diameter, due to the capacity of high deformability of the viscoelastic RBC membrane. The motion and the steady state shape of the RBCs depend on many factors, such as the geometrical parameters of the microvessel through which blood flows, the RBC membrane bending stiffness and the flow velocity. In this study, the effect of the RBC's membrane stiffness on the deformation of a single RBC in a stenosed capillary is comprehensively examined. Smoothed Particle Hydrodynamics (SPH) in combination with the two-dimensional spring network membrane model is used to investigate the motion and the deformation property of the RBC. The simulation results demonstrate that the membrane bending stiffness of the RBC has a significant impact on the RBCs' deformability.

Keywords: Red Blood Cell (RBC), Smoothed Particle Hydrodynamics (SPH), Stenosed Capillary, Meshfree Methods, Microcirculation, Numerical Simulations.

Introduction

RBCs are the most common type of the blood cell in the human blood and they occupy about 45% of total blood volume (Skalak et al. 1989, Tsubota et al. 2006a). Human RBCs consist of a thin viscoelastic membrane and they do not contain nuclei inside of the cell. Due to the existence of the viscoelastic membrane, RBCs exhibit different types of motions and deformed shapes, when the blood flows within the cardiovascular network (Fedosov et al. 2010, Pozrikidis 2003). The motion and the deformation mechanism of a RBC highly depend on the maximum velocity of the plasma flow, bending stiffness of the RBC and the diameter of the microchannel, through which the RBC flows (Shi et al. 2012). Over the last few decades, a number of numerical studies were conducted to understand the RBCs' behaviour in the microchannels.

It is important to study the RBCs' motion and deformation accurately, when they are squeezing through capillaries. Since, some diseases such as malaria, cancer, and sickle cell anemia can alter

the ability of deformability of the RBCs (Jiang et al. 2013), they might not be able to deform enough to pass through the narrow capillaries. Further, if the blood vessel is stenosed, there is a high risk of micro vascular blockage (Cooke et al. 2001). In the past, most of the studies were carried out to investigate the RBCs' behaviour in the microchannels with uniform cross sectional areas and few studies have been done to explore the RBCs' motion and deformation mechanism in stenosed microchannels. Hosseini and Feng (2009) have presented the RBCs' ability of squeezing through a tiny capillary, whose diameter is smaller than the mean diameter of the RBCs. They used the SPH method and modelled the microchannel, such that it has a larger uniform diameter at the inlet and a smaller uniform diameter at the outlet. Vahidkhah and Fatouraee (2012) proposed a immersed boundary–lattice Boltzmann method to investigate the RBCs' behaviour in a stenosed arteriole. However, they presented more qualitative results of the RBCs' deformation in a stenosed arteriole.

The purpose of this paper is to present an advanced numerical modelling technique using SPH to analyse motion and deformation of a single RBC through a stenosed capillary. The RBC membrane is modelled by a spring network and the forces acting on the RBC membrane is determined based on the minimum energy principle (Gallage et al. 2012a, Pan and Wang 2009, Tsubota et al. 2006b). First, we present the motion and deformation of a RBC, when it passes through a stenosed capillary. Then, we compare the effect of the RBC's membrane stiffness on the deformation and the motion of the RBC.

Model and Method

In this study, the RBC membrane is modelled by a two-dimensional spring network as used in the previous studies (Gallage et al. 2012b, Shi et al. 2012). The membrane of the RBC is constructed by 88 membrane particles, which are interconnected by elastic springs. Initially, it is assumed that the shape of the RBC membrane is a circle with radius of 2.8 μm.

$$E_l = \frac{1}{2} K_l \sum_{i=1}^{N} \left(\frac{l_i - l_0}{l_o} \right)^2 \tag{1}$$

$$E_b = \frac{1}{2} K_b \sum_{i=1}^{N} \tan^2 \left(\frac{\theta_i}{2} \right) \tag{2}$$

$$E_s = \frac{1}{2} K_s \left(\frac{s - s_e}{s_e} \right)^2 \tag{3}$$

$$\mathbf{F}_i = -\frac{\partial\left(E_l + E_b + E_s\right)}{\partial \mathbf{r}_i} \tag{4}$$

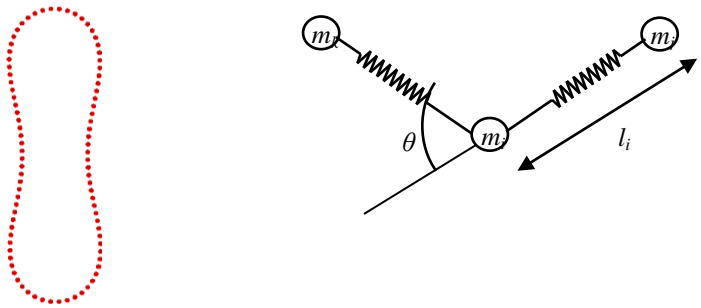

Fig. 1: Spring network model of the RBC

The elastic energy (E_l) stored in the springs due to the stretch/ compression is given by **Eq. (1)** and the elastic bending energy (E_b) stored in the springs due to the bending is given by **Eq. (2)**. In order to maintain a constant membrane area, a penalty function (E_s) is introduced as in **Eq. (3)**. The total force ($\mathbf{F}_i$) acting on the i^{th} membrane particle is calculated, using the principal of virtual work as in **Eq. (4),** where $\mathbf{r}_i$ is the Position vector of the i^{th} Particle. l_i, θ_i, and s are length of the i^{th} spring, angle between two consecutive springs and area of the RBC respectively. Spring constant for stretching/compression (K_l), spring constant for bending (K_b) and penalty coefficient (K_s) are set to 5×10^{-8} N.m, 5×10^{-10} N.m and 1×10^{-5} N.m respectively as used by Shi et al. (2012). The reference length (l_0) is taken as 0.2 μm, while the Equivalent area of the RBC (s_e) is set to $\pi\times(2.8\times10^{-6})^2\times0.55$ m^2 as used in the work by Pan and Wang (2009).When the forces acting on the RBC membrane particles are minimised, the initial circular shape gives a biconcave shape as shown in **Fig. 1.**

RBC internal fluid (cytoplasm) and external fluid (plasma) are modelled by a set of particles and Navier-Stokes equations (**Eq. (5)** and **Eq. (6)**) in Langrangian form are used to model the whole flow field, with the assumption of the system is isothermal.

$$\frac{D\rho}{Dt} = -\rho\nabla\cdot\mathbf{v} \tag{5}$$

$$\frac{D\mathbf{v}}{Dt} = -\frac{1}{\rho}\nabla p + \frac{\mu}{\rho}\nabla^2\mathbf{v} + \mathbf{f} \tag{6}$$

where ρ and μ are the density and the dynamic viscosity of the fluid, $\mathbf{v}$ is the velocity vector and p is the pressure while $\mathbf{f}$ is the vectorial external force.

In SPH methodology, any field function value (f) of a particle can be approximated from the same field function value of surrounding neighbouring particles using a kernel function (W) as shown in

Eq. (7). For this study, popular cubic spline smoothing function is used as used by Gallage et al. (2012b).

$$f_i = \sum_{j=1}^{N} \frac{m_j}{\rho_j} f_j W_{ij} \tag{7}$$

The Navier-Stokes equations are modified according to the SPH methodology (Liu and Liu 2003) and are used to determine the particle positions and velocities. The capillary wall is modelled by a set of boundary particles and pair-wisely repulsive forces are introduced to avoid any penetration of fluid particles through the capillary wall (Gallage et al. 2012b).

The problem domain is discretised into SPH particles, as shown in **Fig. 2**, such that the particle spacing is equal to 0.2 μm. Geometrical parameters of the problem domain is shown in the **Table 1**.

Table 1: Geometrical parameters of the stenosed capillary

Parameter	h_1	h_2	l_1	l_2	l_3	l_4	r_1	r_2	r_3	r_4
Value (μm)	9.8	9.8	4.9	19.6	0.6	9.7	3.7	3.7	3.7	3.7

According to the set geometrical parameters, the total length of the stenosed capillary in x-direction is 45 μm and the minimum height (h_3) at the stenotic area is about 6 μm.

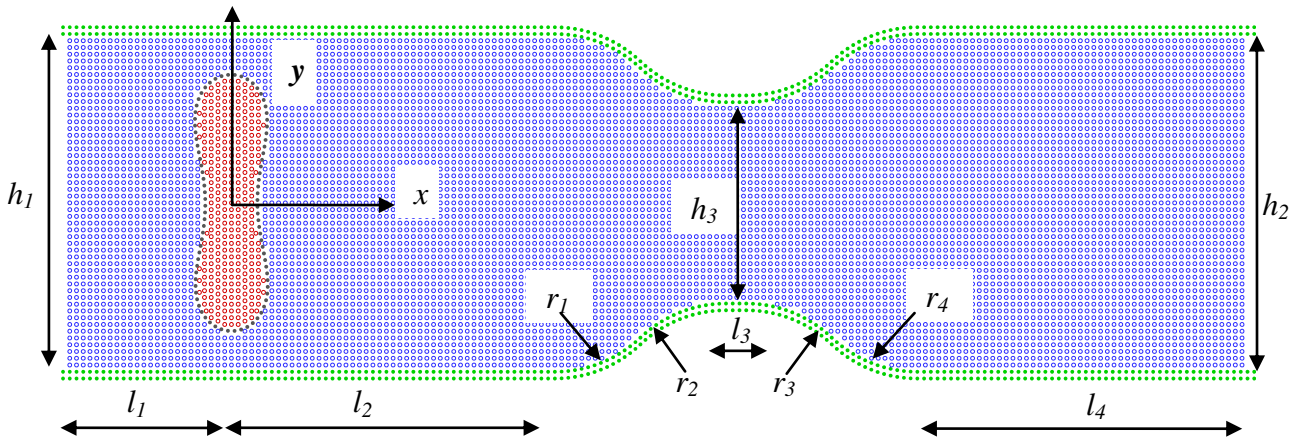

Fig. 2: Initial geometrical configuration of the problem domain

Results and discussions

Deformation Index of the RBC in the stenosed capillary

A constant pressure (P_1=450 Pa) is applied at the inlet, and the outlet pressure is set to zero. Those boundary conditions give a constant pressure gradient of 1×10^7 Pa/m. The pressure of each particle is calculated based on the x-directional distance and the pressure gradient, and then it is applied to the particles. The pressure gradient used for this study is quiet high. If this pressure gradient was applied to a capillary having a uniform diameter of 9.8 μm and no RBCs, then the peak velocity of

the plasma flow would be 0.12005 m/s. It corresponds to Reynolds number, *Re*=1.17649. Due to the applied pressure in the inlet, the RBC begins to move with plasma flow. While RBC is moving it deforms and the initial biconcave shape of the RBC is changed to the parachute shape. **Fig. 3** shows that the deformation of the RBC is quite significant, when it is flowing through the stenosed area.

The Deformation Index of the RBC can be defined as in **Eq. (8)**

$$\mathrm{DI} = \frac{\text{Total length of the RBC } (l)}{\text{Total height of the RBC } (d)} \tag{8}$$

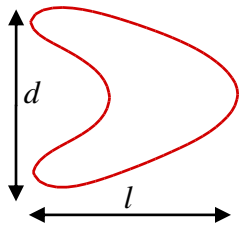

Fig. 3: Deformed RBC; DI= *l*/*d*

Initially, RBC flows through a section where capillary diameter is uniform and during that period of time DI of the RBC increases gradually (see **Fig. 4**). When *t*=0.4 ms, the DI reaches almost a steady value of 0.65. But after *t*=0.4 ms RBC enters to a narrow passage, where cross sectional area of the capillary is suddenly reduced. Then the DI of the RBC increases drastically with time and variation of the DI with the RBC's position shows a similar pattern (see **Fig. 5** and **Fig. 6**). However, it can be seen that from **Fig. 7** the RBC's position does not have a linear relationship with time. The DI reaches a peak value about 1.39 when the RBC squeezes through the stenosed area. This happens at *t*=0.6 ms and a significant difference in the deformed RBC's shape can be observed when it passes through the narrowest area of the capillary (see **Fig 4**). Then the RBC's DI decreases with the time, as it leaves the stenosed area of the capillary and the RBC starts to recover its normal parachute shape again. When the RBC leaves the stenosed area completely, the DI of the RBC gets the almost same value as *t*=0.4 ms. Therefore, the deformation index of the RBC is highly depends on the cross sectional of the capillary, through which RBC moves.

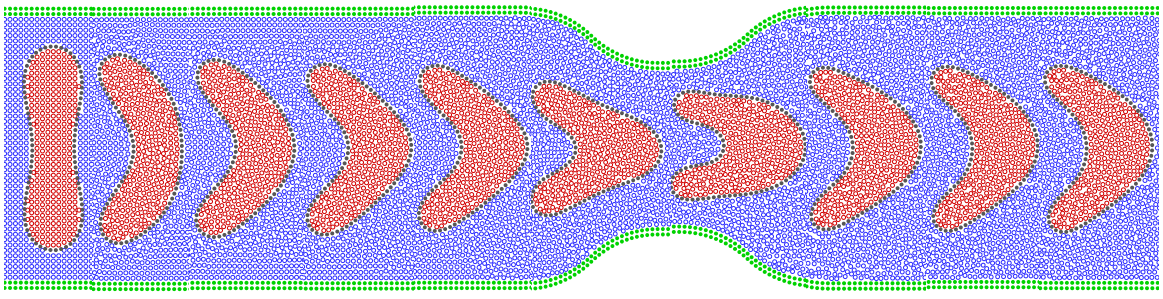

Fig. 4: Deformation of the RBC at *t*=0, 0.1, 0.2, 0.3, 0.4, 0.5, 0.6, 0.7, 0.8 and 0.85 ms

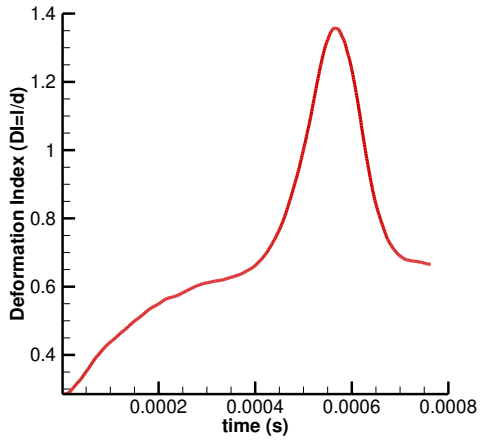

Fig. 5: The variation of the DI with time

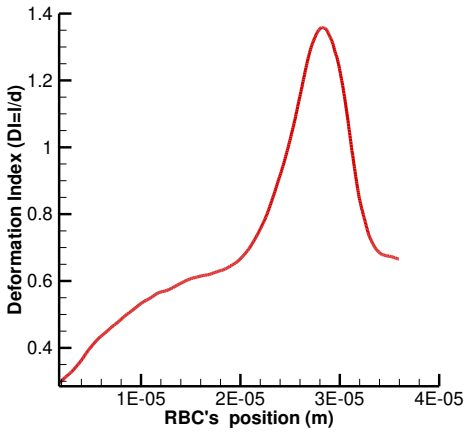

Fig 6.: The variation of the DI with RBC's Position

When the RBC squeezes through the stenosed area, it flows at a maximum velocity of about 0.06 m/s. However, the mean velocity of the RBC takes a lower value just after the stenosed area, compared with its velocity just before the stenosed area (see **Fig. 7**). At t=0.84 ms, all the RBC membrane particles and cytoplasm particles have almost reached a unique velocity (see **Fig. 8**). But, the mean RBC velocity is still subjected to some minor fluctuation, as seen in **Fig. 7**. **Fig. 8** shows that the plasma particles located close to the capillary wall have a lower velocity, while the plasma particle located close to the axis of the capillary (y=0) have a higher velocity.

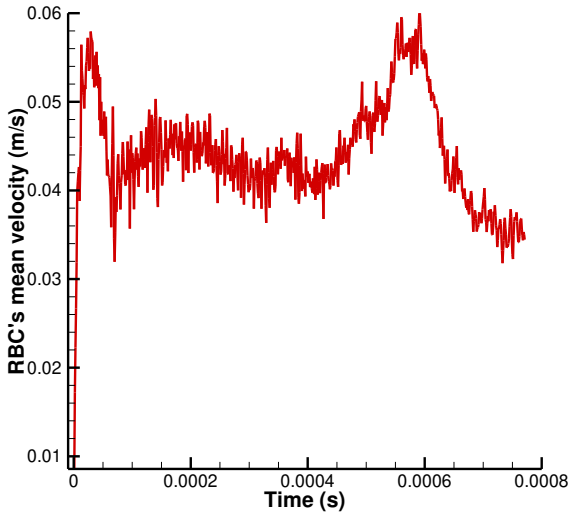

Fig. 7: Variation of RBC's mean velocity

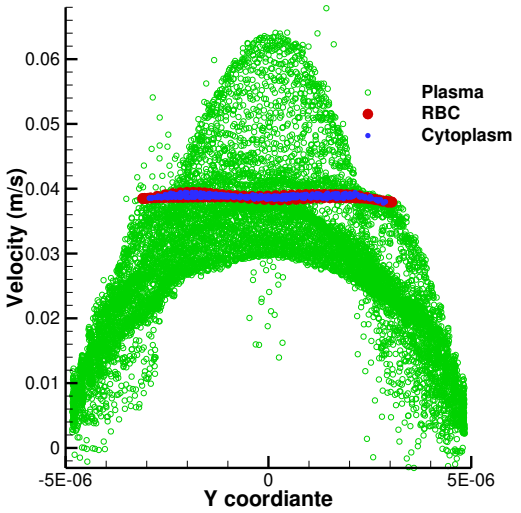

Fig. 8: Velocity profile at t=0.84 ms

Effect of the RBC's membrane stiffness

Deformation Indices of three RBC with different membrane stiffness are compared. For this simulation, l_2 is set to 9.6 μm. Therefore, the total length of the stenosed capillary in x-direction is 35 μm and the minimum height (h_3) at the stenotic area is not changed. P_1 is set to 350 Pa, to

maintain a constant pressure gradient of 1×10^{7} Pa/m. Spring constant for bending (K_b) is changed from 5×10^{-10} N.m to 5×10^{-9} N.m and 5×10^{-11} N.m. All the other simulation parameters are kept same as previous. The RBC having higher K_b value exhibits a lower deformation and the RBC with a less K_b value shows a greater deformation. When the RBC with K_b $=5\times10^{-9}$ N.m flows the stenosed area, the thickness of the plasma layer exist between RBC membrane and the capillary wall is very narrow (see **Fig. 9**). Further increase in bending constant would lead to blockage of the RBC, since RBC deforms less for higher bending constant values. **Fig. 10** shows that three RBCs exhibit similar deformation pattern with respect to their positions. Further, DI of the RBC with K_b=5×10^{-9} has been reduced drastically. While, there is no significant change in the deformation indices of the RBCs with K_b=5×10^{-11} and K_b=5×10^{-10}.

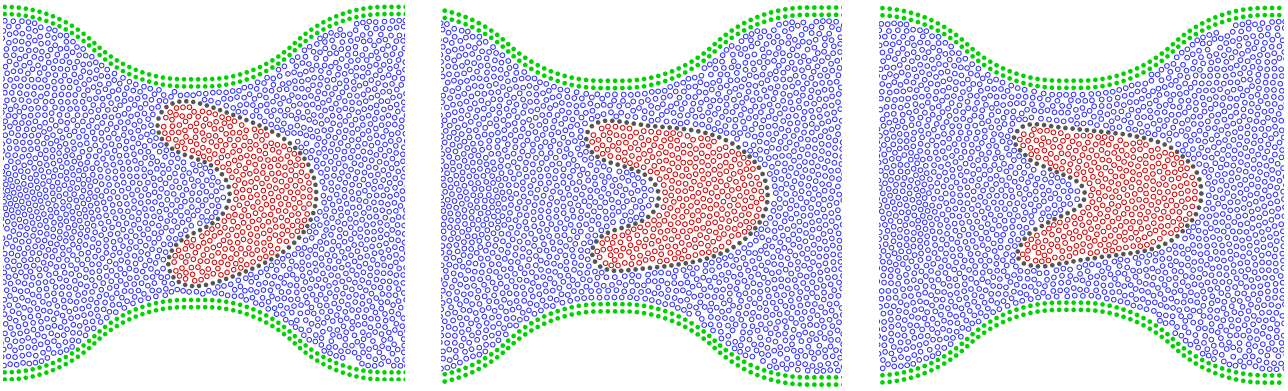

(a) (b) (c)

Fig. 9: Deformed RBC shapes for (a) K_b $=5\times10^{-9}$, (b) 5×10^{-10} and (c) 5×10^{-11} N.m

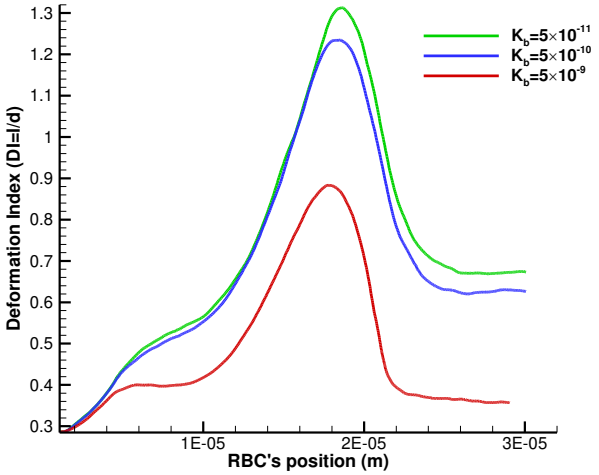

Fig. 10: The variation of the DI with time for different K_b values

Conclusions

The SPH model in combined with the spring network model is used to investigate the RBCs deformation behaviour though a stenosed capillary. We observed that, the geometrical shape of the capillary, through which RBCs move, makes a significant effect on the deformation index of the RBC. When there is a stenosed part in the capillary, the flow field changes and the RBCs are subjected to larger deformation. Further, results revealed that the deformability of the RBCs highly depends on the RBCs bending stiffness. The RBC having a higher bending stiffness shows a less Deformation Index and the thickness of the plasma layer exist between RBC membrane and the capillary wall is very narrow, when the RBC moves through a stenosed capillary. However, to get more accurate results, the deformation property of the RBCs should be studied, when they are interacted with other RBCs. In our future's work, we aim to study the effect of multiple RBCs, when blood is flowing through a stenosed capillary in the near future.

Acknowledgements

Support from the ARC Future Fellowship grant (FT100100172) is gratefully acknowledged.

References

Cooke BM, Mohandas N, Coppel RL. 2001. The malaria-infected red blood cell: structural and functional changes. Advances in parasitology 50: 1-86.

Fedosov DA, Caswell B, Karniadakis GE. 2010. A multiscale red blood cell model with accurate mechanics, rheology, and dynamics. Biophysical journal 98: 2215-2225.

Gallage P, Nayanajith H, Gu Y, Saha SC, Senadeera W, Oloyede A. 2012a. Numerical simulation of red blood cells' motion: a review.

Gallage P, Nayanajith H, Gu Y, Saha SC, Senadeera W, Oloyede A. 2012b. Numerical simulation of red blood cells' deformation using SPH method.

Hosseini SM, Feng JJ. 2009. A particle-based model for the transport of erythrocytes in capillaries. Chemical Engineering Science 64: 4488-4497.

Jiang XM, Wang T, Xing ZW. 2013. Simulation Study of Hemodynamics of Red Blood Cells in Stenotic Microvessels. Advanced Materials Research 647: 321-324.

Liu G-R, Liu M. 2003. Smoothed particle hydrodynamics: a meshfree particle method: World Scientific Publishing Company Incorporated.

Pan TW, Wang T. 2009. Dynamical simulation of red blood cell rheology in microvessels. International Journal of Numerical Analysis & Modeling 6: 455-473.

Pozrikidis C. 2003. Numerical simulation of the flow-induced deformation of red blood cells. Annals of biomedical engineering 31: 1194-1205.

Shi L, Pan TW, Glowinski R. 2012. Deformation of a single red blood cell in bounded Poiseuille flows. Physical Review E 85: 016307.

Skalak R, Ozkaya N, Skalak TC. 1989. Biofluid mechanics. Annual review of fluid mechanics 21: 167-200.

Tsubota K-i, Wada S, Yamaguchi T. 2006a. Particle method for computer simulation of red blood cell motion in blood flow. Computer methods and programs in biomedicine 83: 139-146.

Tsubota K-i, Wada S, Yamaguchi T. 2006b. Simulation study on effects of hematocrit on blood flow properties using particle method. Journal of Biomechanical Science and Engineering 1: 159-170.

Vahidkhah K, Fatouraee N. 2012. Numerical simulation of red blood cell behavior in a stenosed arteriole using the immersed boundary–lattice Boltzmann method. International journal for numerical methods in biomedical engineering 28: 239-256.